Metallophthalocyanines: Versatile Electron-Donating Building Blocks for Fullerene Dyads

Dirk M. Guldi,*,†,‡ Israel Zilbermann,† Andreas Gouloumis,§ Purificación Vázquez,§ and Tomás Torres*,§

Radiation Laboratory, University of Notre Dame, Indiana, 46556, and Departamento de Química Orgánica (C-I), Universidad Autónoma de Madrid, 28049-Madrid, Spain

Received: July 1, 2004; In Final Form: September 9, 2004

A thorough investigation on the physicochemical properties, including electrochemisty and photophysics, of a new class of donor−acceptor hybrids, namely, phthalocyanine-fullerene dyads, consisting of free base **1a** and zinc and copper complexes **1b** and **1c,** respectively, brings new insights into the stabilization of charge-separated radical ion pairs and the impact of redoxactive transition-metal centers on the photoperformance of macrocyclic phthalocyanines. In these dyads, the role of the phthalocyanines is twofold: First, it functions as an antenna (i.e., absorbing very efficiently light in the visible region of the solar spectrum) and, second, as a donor molecule—once photoexcited. The initial photoexcitation is succeeded by an ultrafast electron transfer largely due to the strong electronic coupling between electron donor (Pc) and electron acceptor (C_{60}) generating surprisingly long-lived radical ion pairs $Pc^{\bullet+}-C_{60}^{\bullet-}$ with lifetimes of several nanoseconds. Large driving forces for the charge recombination and small reorganization energies of the Pc−C_{60} ensembles corroborate slow charge recombination dynamics, which, in turn, helps to rationalize the long lifetimes of $Pc^{\bullet+}-C_{60}^{\bullet-}$.

Introduction

In photosynthesis, cascades of short-range energy transfer and electron-transfer events occur between well-arranged organic pigments [i.e., light-harvesting antenna ensemble and photosynthetic reaction center (PRC)] and other cofactors.[1] Thereby, the antenna portion captures light and transduces the resulting excitation energy, via singlet−singlet energy transfer, to the PRC. In the PRC, charges are then separated between several electron acceptor and electron donor units with remarkable efficiency to yield a spatially and electronically well-isolated radical pair. Nowadays, synthetic efforts focus on preparing artificial PRC building blocks en route to efficient nature-mimicking donor−acceptor ensembles.[2] The rational design of such donor−acceptor ensembles capable of light-induced charge separation over long distances on the molecular scale is also a central topic in molecular photovoltaic devices. Toward these ends, ultrafast charge-transfer systems will likely figure prominently in proposed photodriven molecular scale photovoltaics and emerging technologies that focus on light-modulated data storage and retrieval.[3−5]

Phthalocyanines (Pcs),[6] structural analogues of porphyrins, exhibit several outstanding physicochemical properties, which render them of great interest in a variety of scientific and technological areas. Particularly promising appears the use of phthalocyanines in the field of photovoltaics. For example, the strong absorption of phthalocyanines in the solar spectrum with extinction coefficients as high as 200.000 M^{-1} cm^{-1} in the 700-nm range, together with their rich redox chemistry, provides both excellent light-harvesting and electron-donor features and prompts to their potential. Pcs can also function as electron acceptors, which depends, in part, on the Pc's peripheral substitution and the corresponding counterpartner.[7]

In an attempt to establish the potential electronic- and photonic-base cooperation between the two subunits in phthalocyanine-based dyads, we have reported the preparation and study of photophysical properties of systems, in which the phthalocyanine is attached covalently to a variety of photo- and electroactive moieties, like ferrocene, anthraquinone, and $[Ru(bpy)_3]^{2+}$.[8]

Most of the donor−acceptor ensembles that have been synthesized for probing photoinduced electron-transfer processes take advantage of porphyrin derivatives as excited-state electron donors and C_{60} as an electron acceptor because of C_{60}'s remarkable redox (i.e., energetically favorable first reduction step)[9] and structural (i.e., small reorganization energy in electron-transfer processes)[10] properties. Several of these systems[11] retain the characteristic low reorganization energies of fullerenes, which is regarded as one of the key requisites for generating long-lived radical ion pair states. The use of phthalocyanines in C_{60}-based donor−acceptor ensembles is, however, rare,[12−15] despite the long-standing interest in these versatile and unique materials.

We recently communicated[14] that in strongly coupled covalent phthalocyanine-fullerene H_2Pc-C_{60} and $ZnPc-C_{60}$ dyads **1a** and **1b**, respectively, long-lived and highly emissive charge-separated states are formed in condensed media. Importantly, large-driving forces for the charge recombination and small reorganization energies stabilize the radical ion pair state. In these dyads, the phthalocyanine plays the role of an antenna (i.e., absorbing very efficiently light in the visible region of the solar spectrum) and also of a donor molecule.

Moreover, we have also pointed out[15] that in the solid state, the lifetime of the charge-separated state for ZnPc-C_{60}, **1b**, reaches into the millisecond time regime. This is a clear indication that the stabilization of the charge-transfer state—in the solid-state material—is aided by intermolecular interactions.

* To whom correspondence should be addressed. E-mail: D.M.G., guldi.1@nd.edu; T.T., tomas.Torres@uam.es.

† University of Notre Dame.

‡ Current address: Institute for Physical Chemistry, Friedrich-Alexander-Universität Erlanger-Nürnberg, Egerlandstr. 3, D-91058 Erlangen, Germany.

§ Universidad Autónoma de Madrid.

10.1021/jp047105z CCC: $27.50
Published on Web 11/03/2004

CHART 1: Fulleropyrrolidinphthalocyanines MPc (M = H_2, Zn, Cu; 1a−c) and Tetra-*tert*-butylphthalocyanines MPc−C_{60} (M = H_2, Zn, Cu; 6a−c)

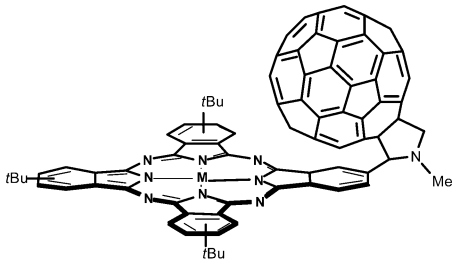

1a M = H_2
1b M = Zn
1c M = Cu

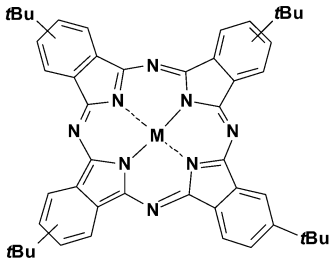

6a M = H_2
6b M = Zn
6c M = Cu

Considering these results, the possibility of using this kind of dyads as materials for photovoltaic devices has come but necessitates first a more thorough investigation and a better understanding of the processes involved. For these reasons, we undertook a more detailed study, which is described herein, on the physicochemical properties reaching from electrochemisty to photophysics of this new class of phthalocyanine−fullerene dyads, including a new hybrid, namely, CuPc−C_{60}, **1c**. **1c** could bring new insights into the stabilization of charge-separated radical ion pairs and the impact of redoxactive transition-metal centers on the photoperformance of macrocyclic phthalocyanines.

Experimental Section

General and Materials. Melting points were determined on a Büchi 504392(S) apparatus and are uncorrected. Infrared spectra were recorded on a Bruker (FT-IR) spectrophotometer. The ^{1}H NMR spectra were obtained on a Bruker AC-300 (300 MHz) and Bruker DRX-500 (500 MHz), and the ^{13}C NMR spectra were obtained on a Bruker AC-300 (75 MHz) and a Bruker DRX-500 (125 MHz) spectrometer. UV−vis spectra were recorded on a Perkin-Elmer 8453 spectrophotometer. The mass spectra (EI and LSIMS) were determined on a VG AutoSpec spectrometer using *m*-NBA as a matrix. The MALDI-TOF mass spectra were determined on a Bruker Reflex III spectrometer. Elemental analyses were performed on a Perkin-Elmer 2400 CHN elemental analyzer. Compounds **6a**−**c** are commercially available.

Electrochemical experiments were conducted with a BAS potentiostat. A glassy carbon electrode was used as working electrode (area 0.07 cm^2), a platinum wire as a counter electrode, and either a silver wire or a pseudo Ag/AgCl electrode (i.e., silver wire in a $KCl_{sat.}/AgCl_{sat.}$ solution all embedded in a Nafion membrane tubing) as a reference electrode. The Fc/Fc^+ couple was used to standardize the reference. Tetrabutylammonium hexafluorophosphate (0.5 M) or tetrahexylammonium hexafluorophosphate (0.05 M) was used as the supporting electrolyte. Picosecond laser flash photolysis experiments were carried out with 532-nm laser pulses from a mode-mode-locked, Q-switched Quantel YG-501 DP Nd:YAG laser system (18 ps pulse width, 2−3 mJ/pulse). Nanosecond laser flash photolysis experiments were performed with laser pulses from a Quanta-Ray CDR Nd:YAG system (532 nm, 6 ns pulse width) in a front face excitation geometry.

Fluorescence lifetimes were measured with a Laser Strope Fluorescence Lifetime Spectrometer (Photon Technology International) with 337-nm laser pulses from a nitrogen laser fiber-coupled to a lens-based T-formal sample compartment equipped with a stroboscopic detector. Details of the Laser Strobe systems are described on the manufactures web site, http://www.pti-nj.com.

Emission spectra were recorded with an SLM 8100 Spectrofluorometer. The experiments were performed at room temperature. Each spectrum was an average of at least five individual scans and the appropriate corrections were applied whenever necessary.

*Tri-tert-butyl-(N-methyl-3,4-fulleropyrrolidin)phthalocyaninatocopper(II) (**1c**).* A well-stirred mixture of tri-*tert*-butylformylphthalocyaninatocopper(II) (**5c**) (46 mg, 0.06 mmol), C_{60} (43 mg, 0.06 mmol), and sarcosine (26.7 mg, 0.3 mmol) in toluene (50 mL) was refluxed under argon for 24 h. After flash chromatography (SiO_2 toluene to ethyl acetate/toluene 1:9) **1c** (37 mg, 41%) (64% based on recovered fullerene) was isolated as a green solid. ^{1}H NMR (500 MHz, $CDCl_3$): δ = 9.1−7.5 (br, 12H), 5.6−5.4, 5.2−5.0, and 4.6−4.4 (br, 3H), 3.2−3.0 (br, 3H), 1.8−1.6 (br s, 27H). IR (KBr): ν = 2955, 1610, 1462, 1388, 1332, 1255, 1140, 1088, 1047, 931, 882 cm^{-1}. UV/vis (*o*-ODCB): λ_{max} (log ϵ) = 344 (5.00), 431 (3.93), 616 (4.61), 685 nm (5.30). MS (MALDI-TOF-dithranol) *m*/*z*: 1519−1523 [*M*+H$^+$].

*Tri-tert-butyliodophthalocyaninatocopper(II) (**3c**).* A mixture of 4-*tert*-butylphthalonitrile (1 g, 5.43 mmol), 4-iodophthalonitrile (**2**) (254 mg, 1 mmol), and $Cu(AcO)_2$ (290 mg, 1.6 mmol) in DMAE (3 mL) was refluxed during 18 h. The solvent was evaporated under reduced pressure, and the crude product was purified by flash column chromatography (SiO_2, toluene/hexane 19:1) to afford **3c** as a blue solid (130 mg, 15%). M.p. > 300 °C. ^{1}H NMR (300 MHz, $CDCl_3$): δ = 8.8−7.2 (br, 12H), 1.7−1.5 (br, 27H). ^{13}C NMR (75 MHz, $CDCl_3$): δ = 153.5, 139.0, 138.0, 128.0, 125.9, 122.5, 36.1, 32.3. IR (KBr): ν = 2955, 1615, 1458, 1394, 1331, 1256, 1144, 1090, 1048, 922, 879 cm^{-1}. UV/vis (*o*-DCB): λ_{max} (log ϵ) = 346 (4.85), 613 (4.61), 682 nm (5.34). MS (MALDI-TOF-dithranol): *m*/*z* 869−873 [*M*+H$^+$]. Anal. calcd for $C_{44}H_{39}N_8CuI$ (870.29): C, 60.72; H, 4.52; N, 12.88 (%). Found: C, 60.38; H, 4.59; N, 12.49 (%).

*Tri-tert-butylvinylphthalocyaninatocopper(II) (**4c**).* A mixture of tri-*tert*-butyliodophthalocyaninatocopper(II) (**3c**) (70 mg, 0.08 mmol) and $Pd(PPh_3)_4$ (4.6 mg, 0.004 mmol) in toluene (50 mL) was stirred under argon. Then, tributyl(vinyl)tin (47 μL, 0.16 mmol) was added and the reaction mixture was heated at 100 °C for 12 h. The solvent was evaporated and the solid residue was triturated with methanol, filtered, and chromatographed (SiO_2, toluene/hexane 19:1) to afford **4c** (54 mg, 88%) as a blue solid. M.p. > 300 °C. ^{1}H NMR (300 MHz, $CDCl_3$): δ = 9.0−7.2 (m, 12H), 7.0−6.8 (m, 1H), 6.2−5.9 (m, 1H), 5.6−5.4 (m, 1H), 1.9−1.7 (m, 27H). ^{13}C NMR (75 MHz, $CDCl_3$): δ = 153.3, 138.2, 135.4, 132.83, 127.6, 122.4, 118.9, 115.2, 36.0, 32.3. IR (KBr): ν = 2955, 2865, 1614, 1505, 1483, 1467, 1396, 1255, 1091, 940, 749 cm^{-1}. UV/vis (*o*-DCB): λ_{max} (log

SCHEME 1: Synthesis of Tri-*tert*-butyl-(*N*-methyl-3,4-fulleropyrrolidin)Phthalocyaninatocopper(II) (1c)

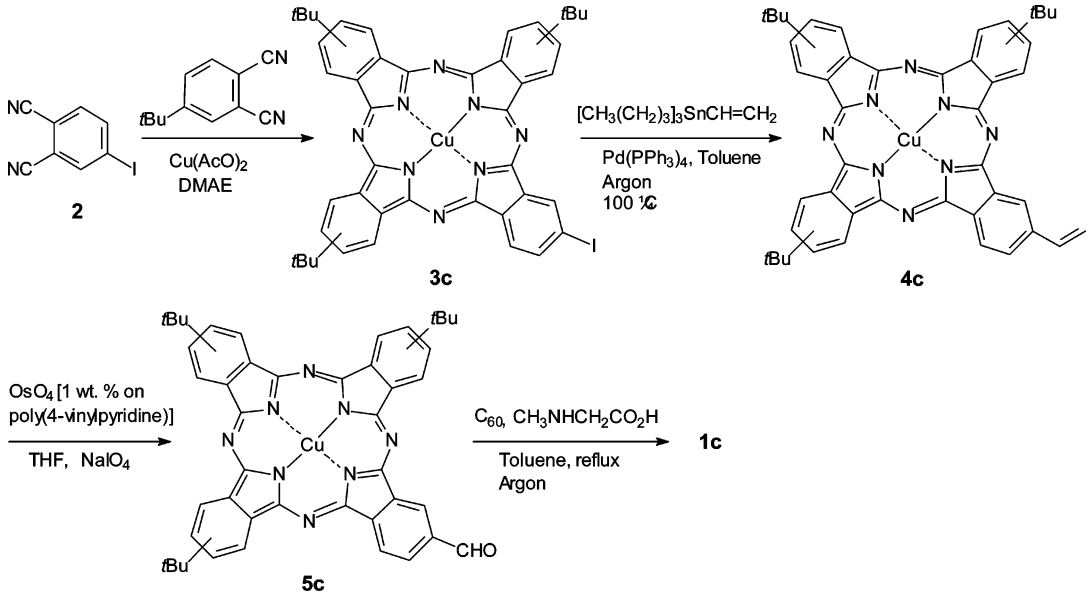

ϵ) = 348 (4.86), 616 (4.56), 683 nm (5.20). MS (MALDI-TOF-dithranol): *m*/*z* 769−772 [*M*+H$^+$]. Anal. calcd for $C_{46}H_{42}N_8$-Cu (770.43): C, 71.71; H, 5.49; N, 14.54 (%). Found: C, 72.10; H, 5.26; N 14.24 (%).

*Tri-tert-butylformylphthalocyaninatocopper(II) (**5c**).* To a suspension of OsO_4 [(200 mg 1wt % on poly(4-vinylpyridine)] and tri-*tert*-butylvinylphthalocyaninatocopper(II) (**4c**) (62 mg, 0.08 mmol) in THF (100 mL) was added dropwise a saturated aqueous solution of $NaIO_4$ (30 mL) at room temperature. The reaction mixture was stirred at this temperature for 16 h, then filtered over Celite, and after the solvents were evaporated under reduced pressure, the crude products were purified by flash chromatography (SiO_2, ethyl acetate/toluene 1:5) to yield **5c** (43 mg, 70%) as a blue solid. M.p. > 300 °C. ^{1}H NMR (300 MHz, $CDCl_3$): δ = 10.2−10.1 (br s, 1H), 9.1−7.2 (m, 12H), 1.8−1.5 (m, 27H). ^{13}C NMR (75 MHz, $CDCl_3$): δ = 190.5, 153.2, 138.3, 134.8, 134.4, 132.9, 131.7, 131.0, 127.6, 123.8, 117.9, 36.1, 32.3. FIT-IR (KBr): ν = 2956, 1696, 1611, 1490, 1398, 1255, 1188, 1080, 955, 746 cm^{-1}. UV/vis (*o*-DCB): λ_{max} (log ϵ) = 348 (4.85), 616 (4.62), 682 nm (5.21). MS (MALDI-TOF-dithranol): *m*/*z* 771−774 [*M*+H$^+$]. Anal. calcd for $C_{45}H_{42}N_8O$ (772.41): C, 69.97; H, 5.22; N, 14.51(%). Found: C, 69.39; H, 5.11; N, 14.37 (%).

Results and Discussion

Metal-free and zinc compounds **1a** and **1b** were prepared according to a previously described procedure.[13] The synthesis of the PcCu−C_{60} system **1c** was carried out in a similar way following the pathway depicted in Scheme 1.

Thus, tri-*tert*-butyliodophthalocyaninatocopper(II) complex (**3c**) was prepared by crossover condensation reaction of 4-*tert*-butylphthalonitrile with 4-iodophthalonitrile (**2**) in the presence of copper(II) acetate under the appropriate conditions in 15% yield, after isolation from the statistical mixture of phthalocyanines by column chromatography on silica gel. A Stille coupling reaction of **3c** using tributyl(vinyl)tin with $Pd(PPh_3)_4$ as catalyst[16] afforded tri-*tert*-butylvinylphthalocyaninatocopper(II) (**4c**) in 88% yield. Formylphthalocyanine **5c** was synthesized by an oxidative cleavage reaction of **4c** using a polymer-supported osmium tetroxide and sodium periodate,[17] as oxidating agents, in 70% yield. The subsequent functionalization of C_{60} was based on the 1,3-dipolar cycloaddition of the azomethine ylide generated in situ from **5c**. The reaction of C_{60} with tri-*tert*-butylformylphthalocyanine **5c** in the presence of an excess of *N*-methylglycine (sarcosine) in refluxing toluene affords the fulleropyrrolidine−phthalocyanine **1c** in 41% yield (64% based on recovered C_{60}). Separation of the dyad **1c** from C_{60} and bisadducts was accomplished by flash chromatography on silica gel using toluene as eluent.

All new compounds were characterized by ^{1}H NMR, ^{13}C NMR, FTIR, and UV/vis spectroscopy, as well as by mass spectrometry, MALDI-TOF (see Experimental Section). The characteristic formyl resonance of compound **5c** appears at about 10.1−10.2 ppm. Multiprotonated isotopic patterns at *m*/*z* 1519−1523 were observed for **1c** in the MALDI-TOF spectrum, along with the corresponding [M−C_{60}]$^+$ fragments, as major species. The ^{1}H NMR spectrum of the dyad **1c** is complicated because of the presence of several regioisomers; however, signals corresponding to the pyrrolidine ring at 5.5, 5.1, and 4.5 ppm can be clearly observed.

Ground-State Features. The UV−vis spectrum in *o*-ODCB of compound **1c** shows a Q-band at 685 nm and a Soret band at 344 nm (Figure 1). A weak absorption at 431 nm is characteristic of the [6,6] monoadduct of C_{60}. The observed slightly red-shift of the Q-band on going from **6c** (682 nm) to **1c** (685 nm) is comparable with what we have found on going from **6a** (666 and 702 nm) to **1a** (670 and 702 nm) and from **6b** (681 nm) to **1b** (683 nm) (all spectra were taken in *o*-DCB as solvent).[13]

To examine the ground-state features of H_2Pc-C_{60} **1a**, ZnPc-C_{60} **1b**, and CuPc-C_{60} **1c**, and to analyze the electronic interactions between the redox- and photoactive moieties, we compared them with their individual building blocks, that is, C_{60}, H_2Pc **6a**, ZnPc **6b**, and CuPc **6c**, in a series of experiments. Starting with electrochemistry, as performed in toluene, *o*-dichlorobenzene/dichloroethane, and benzonitrile, we observed several interesting trends. First, these experiments support the critical notion that the $C_{60}/C_{60}^{\bullet-}$ couple exhibits the strongest electron affinity, while the different Pc/Pc$^{\bullet+}$ couples render clearly the best electron donors. Second, the donor ability increases in the following order: CuPc **1c** < H_2Pc **1a** < ZnPc **1b**. In other words, starting from the free base (i.e., H_2Pc, **6a**) addition of either Cu (i.e., CuPc, **6c**) or Zn (i.e., ZnPc, **6b**) increases or decreases the electron density on the phthalocyanine

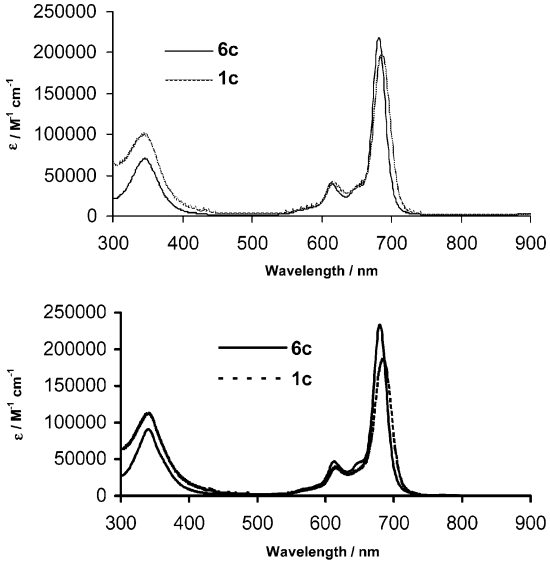

Figure 1. Electronic spectra of CuPc−C60, **1c** (dotted line) and CuPc, **6c** (solid line) in *o*-dichlorobenzene (upper plot) and chloroform (lower plot).

TABLE 1: First Reduction Potentials of Dyads and C_{60} Reference in Variable Solvents

	C_{60}	H_2Pc-C_{60} **1a**	ZnPc−C_{60} **1b**	CuPc−C_{60} **1c**
toluene	−0.63 V	−0.71 V	−0.75 V	−0.69 V
dichoroethane	−0.62 V	−0.66 V[a]	−0.64 V	−0.62 V
benzonitrile	−0.57 V	−0.53 V	−-0.54 V	−0.53 V

[a] *o*-Dichlorobenzene.

macrocycle, respectively. A similar tendency is seen in a related series of complexes with porphyrinic macrocycles. Third, the fullerene reduction in the dyads is, relative to the C_{60} reference, slightly influenced, whose overall level depends on the donor strength of the phthalocyanine: CuPc **1c** < H_2Pc **1a** < ZnPc **1b**. Fourth, a resembling trend is also concluded when inspecting the phthalocyanine oxidation, as depicted in Figure S1. Considering all these facts in common, we must reach the conclusion that in H_2Pc-C_{60} **1a**, ZnPc−C_{60} **1b**, and CuPc−C_{60} **1c** significant ground-state interactions prevail between the electron acceptor and the electron donor subunits of the dyads. A likely rationale is a partial perturbation of the electron densities in the different π-systems, that is, "through-bond" charge-transfer character from the Pc to the C_{60}, which is brought about by their relative short center-to-center separations of around 11 Å.

Importantly, the energy for the radical ion pair $Pc^{\bullet+}-C_{60}^{\bullet-}$ formed, for instance, in a photoinduced electron-transfer reaction (vide infra), decreases in the following order: CuPc−C_{60} **1c** (1.40 eV) > H_2Pc-C_{60} **1a** (1.36 eV) > ZnPc−C_{60} **1b** (1.23 eV); all values are given in benzonitrile and are determined on the basis of the electrochemical investigation.[18] This direct approach for establishing the energetics and thermodynamic driving forces in donor−acceptor systems bears several advantages over applying the widely used "dielectric continuum model".[19] Most importantly, the latter method leads in several cases to large over- or underestimations of the solvent effects. As can be seen from the data gathered in Tables 1 and 2, the energies of the radical ion pairs decrease toward the polar solvents. This observation is well in accord with the presumption that a polar environment provides a better solvation for a charged species, such as the generated fullerene radical anion or phthalocyanine radical cation, than a nonpolar surrounding.

Another sensitive measure for intramolecular interactions is absorption spectroscopy. Generally, the spectra of the three dyads (i.e., H_2Pc-C_{60} **1a**, ZnPc−C_{60} **1b**, CuPc−C_{60} **1c**) absorb strongly across much of the visible region and are dominated by the strong fingerprints of the phthalocyanine chromophores, namely, a high-energy, Soret-type transition around 3.65 eV and a low-energy, Q-band transition around 1.8 eV.[6]

Contributions from C_{60}, whose most intense transitions are found at 220, 265, and 330 nm,[20] are buried within the stronger Soret transitions and come only to light as an overall intensification of the absorption in the UV−vis range. The spectra of the dyads resemble but do not match the sum of the spectra of the component parts: Three fundamental differences are seen when contrasting, for example, CuPc **6c** and CuPc−C_{60} **1c**, which all bear implications in support of intramolecular interactions. First, from the dominant phthalocyanine transitions in **6c** at 345 nm (i.e., Soret-band) and 682 nm (i.e., Q-band), the latter is bathochromically shifted in CuPc−C_{60} **1c** to 685 nm. Second, a lower extinction coefficient is discernible in the phthalocyanine's Q-band: $\log(\epsilon) = 5.34$ at 682 nm (CuPc, **6c**) versus $\log(\epsilon) = 5.30$ at 685 nm (CuPc−C_{60}, **1c**). No absolute comparison can be made for the weaker Soret-band, which in part is due to the absorption of C_{60} moiety in the region of interest, but a similar effect is discernible. Third, the Q-band is subject to a notable broadening for CuPc−C_{60} **1c** relative to CuPc **6c**. Quantitatively similar features were evident in the comparison of the H_2Pc **6a**/H_2Pc-C_{60} **1a** and the ZnPc **6b**/ZnPc−C_{60} **1b** couples, which integrate the same short donor−acceptor linkage.

In ZnPc−C_{60} **1b**, besides the Q-band broadening we see an additional strong absorption feature in a wavelength region where none of the individual components is known to exhibit any meaningful absorptions. Mainly, the low-energy region between 700 and 800 nm is impacted. We assign this additional, low-energy band to a charge-transfer (CT) transition.[21] ZnPc−C_{60} **1b** is the only dyad that shows this feature because of its favorable energetic position—see electrochemistry—while the CT characteristic is absent in H_2Pc-C_{60} **1a** and CuPc−C_{60} **1c**. Two factors are primarily responsible for the lack of spectral resolution. The higher oxidation potentials of the H_2Pc **6a** and CuPc **6c** electron donor (see Tables 1 and 2) relative to ZnPc **6b** results in blue-shifts of the CT transition and, in turn, causes the position to overlap with that of the phthalocyanine's Q-band transition. An additional complication arises from the Q-band location, which is in H_2Pc **6a** and CuPc **6c** red-shifted by about 4−5 nm relative to what is seen for ZnPc **6b**, that is, toward lower energies and toward a possible CT transition. For ZnPc−C_{60} **1b**, the best appreciable CT transitions are seen in chloroform ($\epsilon_{740\ nm} = 8372\ M^{-1}cm^{-1}$) and *o*-dichlorobenzene ($\epsilon_{772\ nm} = 2250\ M^{-1}cm^{-1}$). A demonstration of the CT feature is summarized in Figure 2. With the attributes of the charge-

TABLE 2: First Oxidation Potentials of Dyads 1a, 1b, and 1c and H_2Pc 6a, ZnPc 6b, and CuPc 6c Reference in Variable Solvents

	H_2Pc **6a**	ZnPc **6b**	CuPc **6c**	H_2Pc-C_{60} **1a**	ZnPc−C_{60} **1b**	CuPc−C_{60} **1c**
toluene	+0.96 V	+0.82 V	+1.05 V			+1.1 V
dichoroethane	+0.64 V	+0.58 V	+0.90 V	+0.85 V[a]	+0.67 V	+0.90 V
benzonitrile	+0.74 V	+0.64 V	+0.81 V	+0.83 V	+0.69 V	+0.87 V

[a] *o*-Dichlorobenzene.

TABLE 3: Photophysical Parameters of C_{60} and Pc References in Toluene

	C_{60}	H_2Pc **6a**	ZnPc **6b**	CuPc **6c**
λ_{max}, fluorescence (nm)	715	702	690	not fluorescing
Φ, fluorescence	6.0×10^{-4}	0.67	0.3	not fluorescing
τ, fluorescence (ns)	1.5	6.1	3.6	not fluorescing
λ_{max}, singlet−singlet (nm)	880	860	825	not detected
λ_{max}, triplet−triplet (nm)	700	510	520	500[a]
τ, singlet−singlet (ns)	1.39	5.8	3.3	not detected
τ, triplet−triplet (μs)	20	170	110	0.025[a]
λ_{max}, radical cation (nm)	1000[b]	730, 915 (ref 14)	860 (ref 14)	720[c]

[a] Trip−doublet/trip−quartet excited state. [b] Radical anion feature. [c] Determined by pulse radiolytic oxidation in oxygenated dichloroethane.

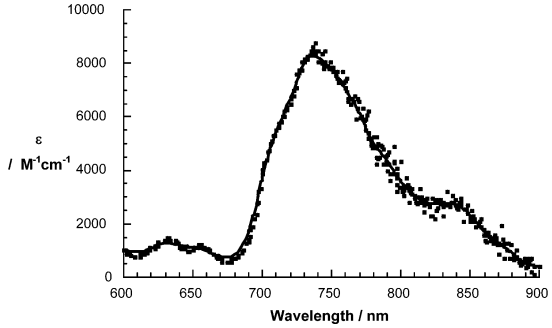

Figure 2. Charge-transfer absorption band of ZnPc−C_{60} **1b** (1.0×10^{-5} M) in room-temperature chloroform solutions. Spectrum is obtained via subtracting the ZnPc **6b** absorption features from those of ZnPc−C_{60} **1b**.

transfer absorption in hand, the electronic coupling elements (V) were estimated via[21]

$$V = \frac{2.06 \times 10^{-2} \sqrt{\epsilon_{max} \nu_{max} \Delta\nu_{1/2}}}{R_{cc}} \qquad (1)$$

in chloroform as 525 cm^{-1} and in *o*-dichlorobenzene as 298 cm^{-1}. The difference in electronic coupling might be ascribed to the energetic position of the CT state, which depends, at least in part, on the solvent polarity. In eq 1, R_{cc} (10.8 Å) denotes the shortest center-to-center separation, ϵ_{max} the extinction coefficient, ν_{max} the energy, and $\Delta\nu_{1/2}$ the half-width of the CT transition.

The conclusion of this section, which deals with ground-state properties of H_2Pc−C_{60} **1a**, ZnPc−C_{60} **1b**, and CuPc−C_{60} **1c**, is a postulate, which infers strong electronic coupling between the Pc and C_{60} subunits. This view is further strengthened by the close donor−acceptor separation, which results from linking the pyrrolidine functionality of the fullerene directly to the phthalocyanine moiety, and for which short center-to-center separations around 11 Å were determined.

Excited-State Features—References. While the photophysics of H_2Pc **6a**, ZnPc **6b**, and C_{60} derivatives are well studied and detailed descriptions for each of them can be found in several authoritative reviews, to the best of our knowledge, no such information is presently available for CuPc **6c**. Thus, we will discuss the photophysics of CuPc **6c** in depth and only refer to those of H_2Pc **6a** and ZnPc **6b** whenever deemed important. All the important data is collected in Table 3.

In typical room-temperature emission experiments (i.e., exclusive excitation either into the Soret- or Q-band region), neither fluorescence nor phosphorescence was seen for CuPc, although H_2Pc **6a** and ZnPc **6b** are both strongly fluorescent probes with quantum yields close to unity (i.e., H_2Pc **6a**: 0.67 and ZnPc **6b**: 0.3). Implicit in the fluorescence silence is an ultrafast deactivation of the initially excited state of this paramagnetic compound, d^9-metal center. A similar mechanism has been proposed for the analogous copper porphyrin (CuP), which showed, however, activation of a moderately strong and long-lived phosphorescence because of thermally equilibrated triplet−doublet/triplet−quartet states.[22] Efficient intersystem crossing, induced by the coupling of the paramagnetic metal center with the normal $\pi-\pi^*$ states of the porphyrin, is responsible for shortening the initial singlet−doublet excited-state lifetime to less than 350 fs. Because of the comparable (i) nature of the porphyrinic and phthalocyaninic macrocycle and (ii) binding of the transition-metal center (i.e., Cu−N), it is likely that a similar ultrafast deactivation pattern governs the photophysics of CuPc **6c**. In contrast, the fluorescence lifetimes of H_2Pc **6a** and ZnPc **6b** are fairly long with values of 6.1 ns and 3.6 ns.

The singlet excited-state energies for H_2Pc **6a** and ZnPc **6b** are 1.73 and 1.79 eV, respectively. Considering the similar ground-state absorption that H_2Pc **6a** and CuPc **6c** show, we can approximate the energy of the initially formed singlet−doublet excited state in CuPc **6c**, which is nonfluorescent, at around 1.73 eV.

Transient absorption spectroscopy proved to be a more suitable tool for our investigation and helped to shed light onto the excited states of all phthalocyanines. Generally, differential absorption spectra of the Pc references in an oxygen-free toluene solution reveal the following features: maxima around 550 nm and minima around 690, which correspond to ground-state bleaching of the Q-band transitions. The transient characteristics are completed by the growth of a near-infrared absorption centered around 820 nm. However, only a single transient is seen for CuPc **6c** on the pico- through microsecond time scale, see Figure S2. H_2Pc **6a** and ZnPc **6b**, on the other hand, give rise to two characteristic metastable states, that is, singlet and triplet excited states, which are both summarized for ZnPc **6b** in Figure 3 (i.e., upper and lower part). Especially, the stability of the CuPc **6c** excited state throughout the picosecond regime is important, since for H_2Pc **6a** and ZnPc **6b** this time window is dominated by intersystem crossing dynamics between the corresponding singlet and triplet manifolds. We like to apply for CuPc **6c**, in analogy to the photochemistry of metalloporphyrins, the convention to assign the transient derived from photoexcitation to thermally equilibrated triplet−doublet/triplet−quartet states.[22] This trip−doublet/trip−quartet state in CuPc **6c** decays by a first-order process with a lifetime of 25 ± 10 ns ($4.0 \pm 1.0 \times 10^7$ s^{-1}), regenerating the doublet ground state. Interestingly, this lifetime is virtually solvent-independent, toluene, *o*-dichlorobenzene, and even benzonitrile showing no effect on the possible coordination of the vacant axial sites, which has been claimed for CuP under concrete experimental conditions, such as a coordinating solvent. A possible rationale for this finding involves the Jahn−Teller distortion of the copper center, which per se weakens the coordination at those axial vacancies. Moreover, none of the studied solvents is a good σ-donor. Because of the overall short-lived nature of this trip−

TABLE 4: Photophysical Parameters of Dyads

feature	solvent	H_2Pc-C_{60} **1a**	$ZnPc-C_{60}$ **1b**	$CuPc-C_{60}$ **1c**
Φ, fluorescence[a,b]	toluene	0.028	0.009	2.2×10^{-5} [c]
	chloroform	0.020	0.0073	2.0×10^{-5} [c]
	o-dichlorobenzene	0.0019	0.0066	1.9×10^{-5} [c]
	benzonitrile	0.017	0.0055	1.2×10^{-5} [c]
λ_{max}, CT fluoresence (nm)	toluene	796	770	not detected
	chloroform	793	777	
	o-dichlorobenzene	803	809	
	benzonitrile	810	821	
τ, CT fluorescence (ns)	toluene	5.5	3.1	not detected
	chloroform		3.05	
	o-dichlorobenzene	5.1	2.7	
	benzonitrile	3.9	2.3	
τ, excited state (ps)	toluene	$\leq$20	$\leq$20	35
	THF	35		
	benzonitrile	29		
τ, $Pc^+-C_{60}^-$ transient (ns)	toluene	5.8	3.1	
	chloroform		3.05	
	THF	4.6	2.87	7.8
	benzonitrile	3.1	2.29	4.8
Φ, triplet	toluene		0.65	0.75
	chloroform	no excited-state product	0.19	0.04
	o-dichlorobenzene	state product	0.07	0.04
	benzonitrile		0.03	0.03

[a] Excitation at 670. [b] Measured at ~700 nm M. [c] Residual C_{60} fluorescence, which occurs in the same spectral region.

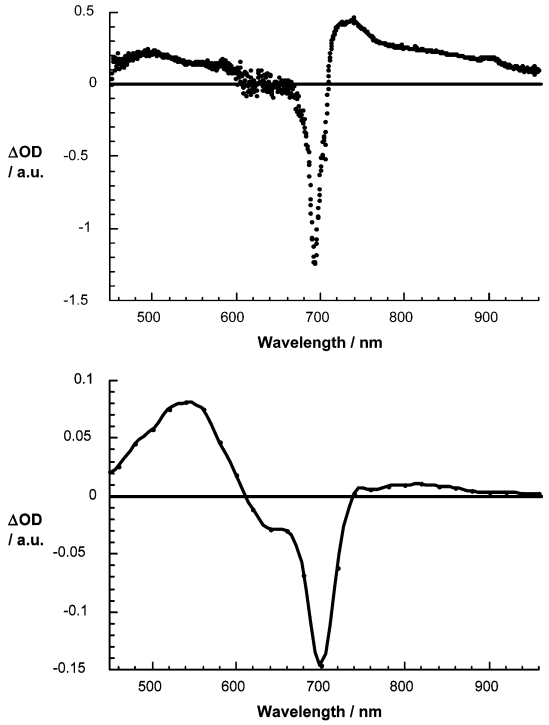

Figure 3. Differential absorption spectrum (visible and near infrared) obtained upon picosecond (upper plot) and nanosecond (lower plot) flash photolysis (355 nm) of ~1.0×10^{-5} M solutions of ZnPc **6b** in nitrogen-saturated THF with a time delay of 100 ps and 100 ns, respectively. The spectral changes reflect the singlet and triplet excited-state features of ZnPc.

doublet/trip−quartet state, molecular oxygen exerts no meaningful impact. By contrast, the triplet states for ZnPc **6b** (1.2 eV) and H_2Pc **6a** (1.24 eV) have much longer lifetimes of around 110 μs for the former and slightly longer values of 170 μs for the latter. Both species disclose nearly diffusion-controlled rate constants (i.e., toluene: ~10^{-9} $M^{-1}s^{-1}$) in their reaction with molecular oxygen to yield singlet oxygen. Formation of singlet oxygen was independently confirmed by following the phosphorescence fingerprint in the near-infrared region at 1265 nm.

A final word should address the question related to the energy of the CuPc's trip−doublet/trip−quartet state. This is rather important within the context of evaluating the driving forces for intramolecular energy and electron-transfer reactions. As an upper estimate, we like to use the value determined for CuP (1.63 eV), which is certainly overstated, while a lower estimate would be close to that of the charge-separated state, $CuPc^{\bullet+}-C_{60}^{\bullet-}$, that is, as low as 1.52 eV in benzonitrile.

Emission Features of Dyads. Preliminary insight into conceivable electron-transfer implications was lent from steady-state fluorescence experiments. The data are always set in relation to the reference compounds, which lack the counterpart, see previous section. The lack of emissive response for the CuPc **6c** chromophore hampers a meaningful analysis of $CuPc-C_{60}$ **1c**. However, excitation in the near-visible region opened the way to probe at least the fullerene singlet excited state, whose energy (1.76 eV) and quantum yield (6.0×10^{-4}) is well known. At 300 nm, the fullerene contribution accounts for nearly 70% of the dyad's absorption. In fact, this approach turned out to be successful. As can be seen from Table 4, which summarizes the fullerene fluorescence quantum yields, a notable quenching of the fullerene fluorescence is observed. In toluene, the quenching reaches a factor of 27 relative to a fulleropyrrolidine reference. Upon modifying the solvent polarity from toluene ($\epsilon = 2.38$) via chloroform ($\epsilon = 4.8$) and *o*-dichlorobenzene ($\epsilon = 9.98$) to benzonitrile ($\epsilon = 24.8$), a gradual intensification of the quenching is discernible.

This observation is in line with the thermodynamic driving force ($-\Delta G_{CS}^{\circ} \sim 0.36$ eV in benzonitrile) for a charge-transfer reaction evolving from the fullerene singlet excited state.

Relative to the ZnPc **6b** and H_2Pc **6a** fluorescence, we found the emission of the $ZnPc-C_{60}$ **1b** and H_2Pc-C_{60} **1a** dyads red-shifted to 698 and 710 nm, respectively, and their quantum yield reduced (Figure 4). In nonpolar toluene, the quantum yields are as low as 0.009. In polar solvents, the quantum yields are further decreased and reach values as low as 0.0055, see Table 4. No discernible band due to the fullerene emission is evident, though any such emission would be largely obscured by the overlapping features of the phthalocyanine emission spectrum. From the solvent dependence, we again infer an efficient electron-transfer

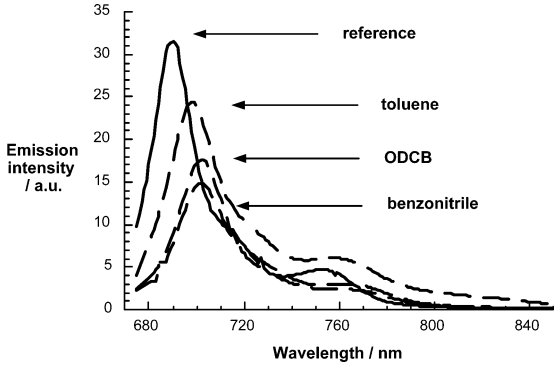

Figure 4. Emission spectra of ZnPc **6b** reference in toluene (solid line) and ZnPc−C_{60} **1b** dyad in different solvents (see labels for assignment) with matching absorption at the 660-nm excitation wavelength $OD_{680nm} = 0.8$. The emission spectra of ZnPc−C_{60} **1b** were amplified; the absolute difference, for example, in toluene between ZnPc **6b** and ZnPc−C_{60} **1b** is 33.

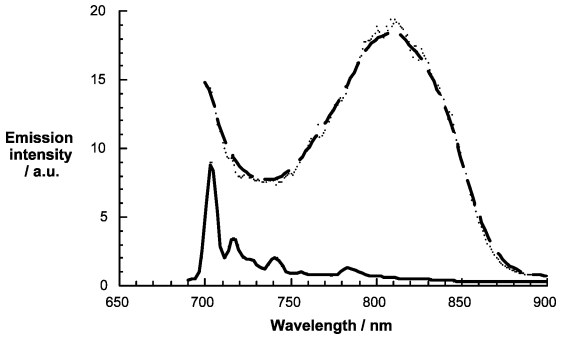

Figure 5. Fluorescence spectra of ZnPc−C_{60} **1b** (solid line) in *o*-dichlorobenzene and C_{60} reference (dotted line) at 77 K with matching absorption at the 670-nm excitation wavelength.

quenching of the locally excited H_2Pc **6a** and ZnPc **6b** chromophores. Further support for this argument comes from the energy gap ($-\Delta G_{CS}°$), associated with charge-separation, as a function of solvent polarity (ϵ), see Table S4. The energies of the charge-separated state lie notably below those of the three singlet excited states, that is, ^{1}*H_2Pc (**1a**) (1.73 eV), ^{1}*ZnPc (**1b**) (1.79 eV), and ^{1}*C_{60} (1.76 eV), which suggest a strongly exothermic electron transfer in both instances to form $H_2Pc^{\bullet+}$−$C_{60}^{\bullet-}$ and $ZnPc^{\bullet+}$−$C_{60}^{\bullet-}$, see below.

A closer inspection of the H_2Pc−C_{60} **1a** and ZnPc−C_{60} **1b** emission spectra reveals a substantial broadening. Although fullerenes typically fluoresce in the range of the spectral broadening, these contributions can be ruled out, bearing in mind the low yields ($\Phi = 6.0 \times 10^{-4}$).[20] In line with the assumption that the width of the charge-transfer emission relates to $(4\lambda_S k_B T)^{1/2}$, lowering the temperature to 77 K helped to convolute the emission bands, which are broad at room temperature.[23] The detection of the charge-transfer emission is not limited to toluene, even using polar media leads to similar features. An illustrative example is given in Figure 5, which shows a maximum at 809 nm for the *o*-dichlorobenzene case, together with the fluorescence spectra of a suitable C_{60} reference. The energy difference between absorption and emission is small: the values are 0.08 eV (chloroform) and 0.075 eV (*o*-dichlorobenzene). Considering that the energetic differences nearly equal $2\lambda_V$, we can estimate the reorganization energy (λ_V) to 0.04 ± 0.01 eV in both solvents. This suggests that any influence of the solvent on the charge-transfer parameters relates to changes in the outer-sphere reorganization energy. Evidence for this hypothesis comes from the following observation: The position of the charge-transfer band is given by $-(\lambda_S + \Delta G_{CR}°)$

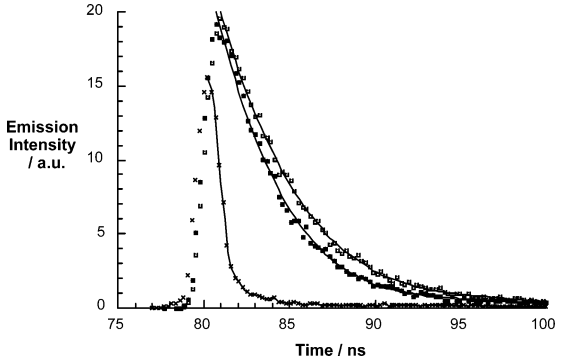

Figure 6. Time-resolved fluorescence decay of ZnPc **6b** (open circles) and ZnPc−C_{60} **1b** (closed circles) in room-temperature toluene solutions (1.0×10^{-5}); 337-nm excitation wavelength, 698-nm monitoring wavelength, crosses represent the laser scatterer.

as the transition occurs downward to the lowest vibrational level of the singlet ground state. λ_S-values of 0.32 ± 0.01 eV result for ZnPc−C_{60} **1b** in chloroform and also in *o*-dichlorobenzene.

On the basis of the low fluorescence quantum yields of the fullerene singlet excited states 6.0×10^{-4}, probing near-visible light excitation in H_2Pc−C_{60} **1a** and ZnPc−C_{60} **1b** renders extremely difficult. In part, the H_2Pc **6a** and ZnPc **6b** fluorescence, which coincides energetically with that of C_{60}, is even in the dyads with values about 10^{-3} still appreciably stronger than that of the unquenched C_{60}.

An independent probe for the magnitude of electron-transfer quenching is fluorescence lifetime experiments. Thus, to complement the steady-state studies and resolve the deactivation dynamics of the photoexcited ^{1}*H_2Pc **6a** and ^{1}*ZnPc **6b**, solutions of the corresponding dyads were probed by time-resolved fluorescence decay measurements and compared with those of the references. In ZnPc−C_{60} **1b**, the emission lifetime of the 698-nm component fits to a first-order rate law with values ranging between 3.6 and 2.3 ns. Even larger values were determined for the H_2Pc−C_{60} **1a** fluorescence at 710 nm: 5.5−3.9 ns. In Figure 6 we compare, for example, the 698-nm fluorescence for ZnPc−C_{60} **1b** with that of ZnPc **6b**. Interestingly, within the accuracy of our instrumental response, which is ca. 100 ps, we could not detect any short-lived component. These extremely long fluorescence lifetimes are surprising considering that from steady-state experiments a difference of ~50 emerges between the fluorescence of the dyads and those of the references. To rule out intermolecular effects, concentration dependences of the fluorescence features were run in each case and in several solvents. Probing dyad concentrations between 3.5 and 65 μM, both quantum yields and lifetimes are virtually constant. The maximum deviation that we found in these experiments (i.e., steady-state and time-resolved) was less than 5%. Taken all the results into concert, we must conclude that the origin of the long-lived emission is not the locally excited ^{1}*H_2Pc **6a** state or ^{1}*ZnPc **6b**, but a low-lying charge-transfer state. For the CuPc−C_{60} **1c** dyad, we recorded the 715-nm maximum of the fluorescence in fulleropyrrolidines. The C_{60} reference reveals nearly solvent-independent fluorescence lifetimes (τ) of 1.5 ns. The only observable feature that changes in room-temperature emission measurements is the maximum, which discloses a moderate red-shift of around 5 nm when moving from toluene toward more polar environments. When, however, inspecting the CuPc−C_{60} **1c** dyad, no detectable C_{60} fluorescence was registered. The following relation:

$$k = 1/\tau_{(dyad)} = [\Phi_{(ref)} - \Phi_{(dyad)}]/[\tau_{(ref)}\,\Phi_{(dyad)}] \qquad (2)$$

SCHEME 2: Energy Levels in Photoexcited ZnPc−C_{60} 1a, Toluene

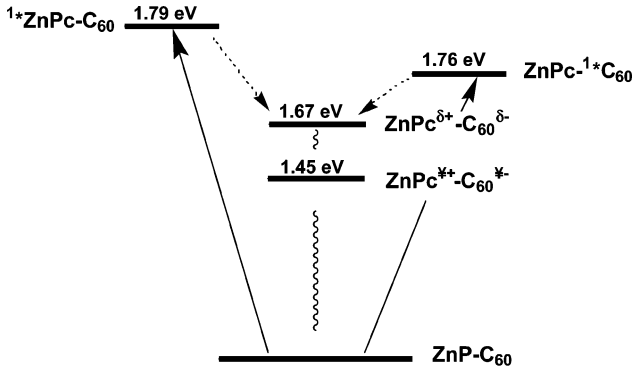

allows us to extrapolate rate constants for the intramolecular deactivation about 2×10^{10} s^{-1}, which is faster than our instrumental time response of 100 ps. On this basis, we can rationalize the absence of C_{60} fluorescence in our experiments.

Transient Absorption Features of Dyads. In summary, steady-state and time-resolved fluorescence measurements infer that a solvent-dependent and rapid electron transfer prevails in H_2Pc−C_{60} **1a** and ZnPc−C_{60} **1b**. To shed light (i) on the mechanism by which the Pc's subunit singlet excited state in the dyads is deactivated and (ii) on the nature of the product, evolving from this intramolecular deactivation, complementary transient absorption measurements were necessary (i.e., with picosecond through millisecond time resolution). Following the time evolution of the characteristic singlet excited state features of Pc's and especially those of CuPc **6c** is a convenient mode to identify spectral features of the resulting photoproducts and to determine absolute rate constants for the intramolecular decay.

In CuPc−C_{60} **1c**, the transients at early times (i.e., 20 ps) are practically identical to those of the CuPc **6c** reference, exhibiting a trip−doublet/trip−quartet state absorption around 825 nm, see Figure S2. Instead of the slow decay dynamics ($4.0 \pm 1.0 \times 10^7$ s^{-1}), the lifetime of the trip−doublet/trip−quartet state is governed by a rapid intramolecular decay. From fitting the decay time profiles, we determined rates about $\sim 2 \times 10^{10}$ s^{-1}. Notably, these values are in excellent agreement with the extrapolation of the fluorescence data. The transient absorption changes, recorded at the conclusion of the fast deactivation, show a sharp peak around 720 nm, the characteristic near-infrared fingerprint of the one-electron oxidized CuPc$^{\bullet+}$, and are shown in Figure 7. As far as the C_{60} moiety is concerned, a transient maximum in the near-infrared around 1000 nm (not shown) corroborates the reduction of the electron acceptor.

For H_2Pc−C_{60} **1a** and ZnPc−C_{60} **1b**, the decay kinetics of the initial singlet excited states (i.e., ^{1}*H_2Pc−C_{60} **1a** and ^{1}*ZnPc−C_{60} **1b**) were not resolved, since they deactivate essentially instantaneous on our picosecond time scale (i.e., 20 ps). Relative to CuPc−C_{60} **1c**, the faster kinetics can be understood on the basis of the much larger energy gaps for the intramolecular charge separation processes ($-\Delta G_{CS}°$) in H_2-Pc−C_{60} and ZnPc−C_{60}, see Table S4. Instead, we estimated a lower limit for the charge-transfer kinetics, which are essentially that of our instrumental response ($\sim 5 \times 10^{10}$ s^{-1}).[24] Transient characteristics of the one-electron oxidized radical cation, that is, ZnPc$^{\bullet+}$ and H_2Pc$^{\bullet+}$, are maxima at 860 and 915 nm, respectively. Figure 8 compares the radical cation spectra of ZnPc$^{\bullet+}$ and H_2Pc$^{\bullet+}$.

The decay curves of both fingerprints, that is, Pc$^{\bullet+}$ and $C_{60}^{\bullet-}$, fit closely to a single-exponential decay. More importantly, the lifetimes of a few nanoseconds resemble those seen for the

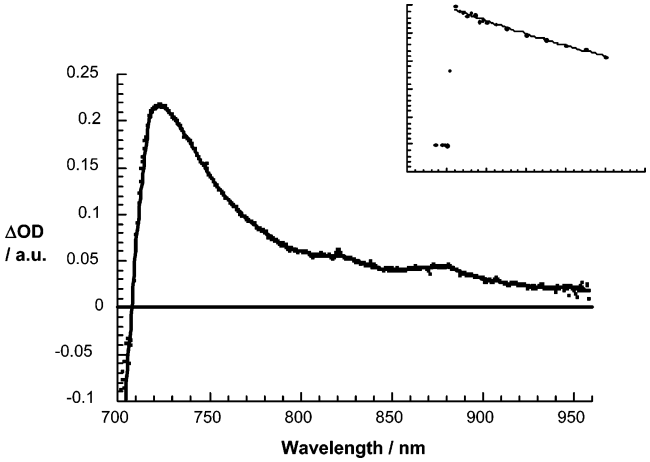

Figure 7. Differential absorption spectrum (visible and near infrared) obtained upon picosecond flash photolysis (355 nm) of $\sim 1.0 \times 10^{-5}$ M solutions of CuPc−C_{60} **1c** dyad in nitrogen-saturated THF with a time delay of 500 ps at room temperature. The spectral changes reflect the one-electron-oxidized π-radical cation features of CuPc. Insert shows decay profile for radical pair in CuPc−C_{60} **1c** at 860 nm.

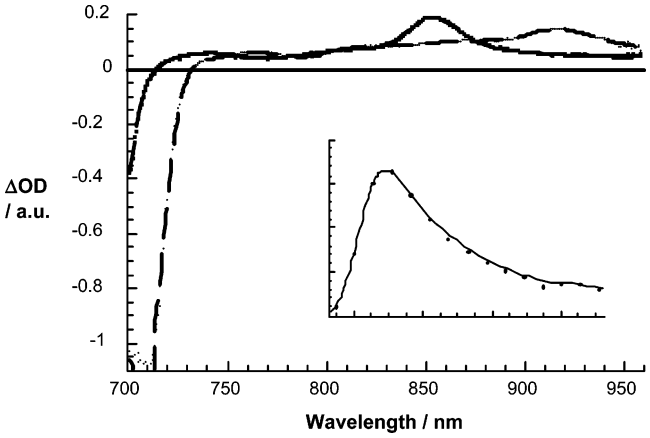

Figure 8. Differential absorption spectrum (visible and near infrared) obtained upon picosecond flash photolysis (355 nm) of $\sim 1.0 \times 10^{-5}$ M solutions of H_2Pc−C_{60} **1a** (dashed line) and ZnPc−C_{60} **1b** (solid line) dyad in nitrogen-saturated benzonitrile with a time delay of 500 ps at room temperature. Insert shows decay profile for radical pair in ZnPc−C_{60} **1b** at 860 nm.

charge-transfer emission in H_2Pc−C_{60} and ZnPc−C_{60}, see Table 4. The dependence of k_{CR} versus free-energy changes indicates stabilizing effects for the charge-separated state at higher $-\Delta G_{CR}°$ values. These are clear attributes describing the inverted region of the classical Marcus-parabola.[25] In the next step, we analyzed the driving force dependence on the rate constants, by applying eq 3, in which V represents the electronic coupling matrix element.

$$k_{ET} = \left(\frac{4\pi^3}{h^2 \lambda k_B T}\right)^{1/2} V^2 \exp\left[-\frac{(\Delta G_{ET}{}^0 + \lambda)^2}{4\lambda k_B T}\right] \qquad (3)$$

For our current analysis, we transferred eq 3 to a linear expression (i.e., eq 4).

$$k_B T \ln k_{ET} + \frac{\Delta G_{ET}{}^0}{2} = k_B T \ln\left[\left(\frac{4\pi^3}{h^2 \lambda k_B T}\right)^{1/2} V^2\right] - \frac{\lambda}{4} - \frac{(\Delta G_{ET}{}^0)^2}{4\lambda} \qquad (4)$$

The driving forces ($-\Delta G_{ET}°$) were determined on the basis of the first oxidation potential of the Pc donor and the first reduction potential of the fulleropyrrolidine. In line with eq 4, $[k_BT \ln k_{ET} + (\Delta G_{ET}°/2)]$ versus $(\Delta G_{ET}°)^2$ gives a linear correlation, see Figure S3. The reorganization energies (λ) and electronic coupling (V) values are obtained as 0.73 eV and 23 cm^{-1}, respectively.

To further examine the charge-recombination dynamics, the same dyad solutions were excited with a 6-ns laser pulse. For CuPc−C_{60}, the lack of any residual absorption suggests that charge recombination regenerates the doublet ground state qualitatively. This observation is in line with a simple thermodynamic evaluation. Once formed, there is no real state between the radical pair state, $CuPc^{•+}-C_{60}^{•-}$, and the doublet ground state, which could be populated. The picture is, however, quite different for ZnPc−C_{60} and H_2Pc−C_{60}. In fact, after the conclusion of the 6-ns laser pulse, features were noted that resemble the triplet excited states of the chromophores. Via the comparative method, we measured the triplet quantum yields, which are listed in Table 4. As can be seen, the Pc's triplet evolves as a relatively high-yield product of charge recombination in nonpolar solvents. In polar solvents, the quantum yields are marginally small, but still detectable. We have to consider a competitive scenario between ground-state reinstatement and triplet formation. The fact is that in polar environments the triplet yields drop although this process is energetically still feasible. For sure, the large driving forces ($-\Delta G_{CR}° > 1.23$ eV) for the direct pathway, namely, reconstitution of the ground state, suggest dynamics that are deeply buried in the inverted region. The driving forces for the triplet formation, on the other hand, are generally very small ($-\Delta G_{CR}° \sim 0.3$ eV) and are located in the normal region. Once we move to a more polar solvent, we lower the energy of the charge-separated state and, consequently, both energy gaps become smaller. Because of its inverted behavior, the ground-state repopulation is accelerated and, in turn, wins over the triplet formation, which is located in the normal region of the Marcus parabola, leading to slower rates.

Conclusions

A series of phthalocyanines, that is, free base (H_2Pc), zinc (ZnPc), and copper (CuPc), are probed as antenna molecules in new donor−acceptor hybrids. The initial photoexcitation is succeeded by an ultrafast electron transfer largely because of the strong electronic coupling between electron donor (Pc) and electron acceptor (C_{60}) generating surprisingly long-lived radical ion pairs $Pc^{•+}-C_{60}^{•-}$ with lifetimes of several nanoseconds. However, we like to refer to some recent findings in C_{60}-based dyads that indicated under particular circumstances even longer lifetimes.[26]

Important in the current case is that the one-electron oxidized product of the phthalocyanines is always the ligand-centered π-radical cation, despite, for instance, the redoxactivity of the copper center in CuPc. Besides small reorganization energies of the Pc−C_{60} ensembles, large driving forces for the reconstitution of the ground state corroborate charge-recombination dynamics that are deeply buried in the inverted region and, in turn, helps to rationalize the long lifetimes of $Pc^{•+}-C_{60}^{•-}$.

Acknowledgment. The authors are grateful for the financial support of the CICYT and Comunidad de Madrid (Spain) and the European Union through Grants BQU2002-04697, 07N/0030/2002, and HPRN-CT-2000-0127, respectively. Part of this work was supported by the Office of Basic Energy Sciences of the U.S. Department of Energy. This is contribution NDRL-4561 of the Radiation Laboratory. I.Z. acknowledges sabbatical leave from the Nuclear Research Center Negev, Beer Sheva, Israel.

Supporting Information Available: Cyclic voltammogram of ferrocene, 1a, and 1c, differential absorption spectrum of 6c, plot of $[k_BT \ln k_{ET} + (\Delta G°_{ET}/2)]$ vs $(\Delta G°_{ET})^2$, energies of states and thermodynamic driving forces. This material is available free of charge via the Internet at http://pubs.acs.org.

References and Notes

(1) (a) *The Photosynthetic Reaction Center;* Deisenhofer, J., Norris, J. R., Eds.; Academic Press: New York, 1993. (b) *Molecular Mechanisms of Photosynthesis*; Blankenship, R. E., Ed.; Blackwell Science, 2002.

(2) (a) *Electron Transfer in Chemistry;* Balzani, V., Ed.; Wiley-VCH: Weinheim, Germany, 2001. (b) Turro, N. J. *Modern Molecular Photochemistry*; University Science Books: Mill Valley, CA, 1991; pp 321−361. (c) Speiser, S. *Chem. Rev.* **1996**, *96*, 1953−1976.

(3) (a) Gust, D.; Moore, T. A.; Moore, A. L.; Lee, S.-J.; Bittersmann, E.; Luttrull, D. K.; Rehms, A. A.; DeGraziano, J. M.; Ma, X. C.; Gao, F.; Belford, R. E.; Trier, T. T. *Science* **1990**, *248*, 199−201. (b) Gust, D.; Moore, T. A.; Moore, A. L.; Macpherson, A. N.; Lopez, A.; DeGraziano, J. M.; Gouni, I.; Bittersmann, E.; Seely, G. R.; Gao, F.; Nieman, R. A.; Ma, X. C.; Demanche, L. J.; Hung, S.-C.; Luttrull, D. K.; Lee, S.-J.; Kerrigan, P. K. *J. Am. Chem. Soc.* **1993**, *115*, 11141−11152. (c) Bennett, I. M.; Farfano, H. M. V.; Bogani, F.; Primak, A.; Liddell, P. A.; Otero, L.; Sereno, L.; Silber, J. J.; Moore, A. L.; Moore, T. A.; Gust, D. *Nature* **2002**, *420*, 398−401.

(4) (a) Balzani, V.; Credi, A.; Raymo, F. M.; Stoddart, J. F. *Angew. Chem., Int. Ed.* **2000**, *39*, 3348−3391. (b) Balzani, V.; Credi, A.; Venturi, M. In *Stimulating Concepts in Chemistry;* Vögtle, F., Stoddart, J. F., Shibasaki, M., Eds.; Wiley-VCH: Weinheim, Germany, 2000.

(5) (a) Yu, G.; Gao, J.; Hummelen, J. C.; Wudl, F.; Heeger, A. J. *Science* **1995**, *270*, 1789−1791. (b) Granström, M.; Petritsch, K.; Arias, A. C.; Lux, A.; Andersson, M. R.; Friend, R. H. *Nature* **1998**, *395*, 257−260. (c) Brabec, C.; Sariciftci, N. S.; Hummelen, J. C. *Adv. Funct. Mater.* **2001**, *11*, 15−26.

(6) (a) *Phthalocyanines: Properties and Applications*; Leznoff, C. C., Lever, A. B. P., Eds.; VCH: Weinheim, Germany, 1989, 1993, 1996; Vols. 1−4. (b) Hanack, M.; Heckmann, H.; Polley, R. In *Methods in Organic Chemistry (Houben-Weyl)*; Schaumann, E., Ed.; Thieme: Stuttgart, 1998; Vol. E 9d, p 717. (c) de la Torre, G.; Nicolau, M.; Torres, T. In *Phthalocyanines: Synthesis, Supramolecular Organization and Physical Properties (Supramolecular Photosensitive and Electroactive Materials);* Nalwa, H. S., Ed.; Academic Press: New York, 2001. (d) Rodríguez-Morgade, M. S.; de la Torre, G.; Torres, T. In *The Porphyrin Handbook*; Kadish, K. M., Smith, K. M., Guilard, R., Eds.; Academic Press: San Diego, CA, 2003; Vol. 13. (e) G. de la Torre, P.; Vázquez, F.; Agulló-López; Torres, T. *Chem Rev.* **2004**, *104*, 3723−3750.

(7) Martínez-Díaz, M. V.; Esperanza, S.; de la Escosura, A.; Catenalli, M.; Yunus, S.; Luzzati, S.; Torres, T. *Tetrahedron Lett.* **2003**, *44*, 8475−8478.

(8) (a) González-Cabello, A.; Vázquez, P.; Torres, T. *Tetrahedron Lett.* **1999**, *40*, 3263−3266. (b) Gouloumis, A.; Liu, S.-G.; Vázquez, P.; Echegoyen, L.; Torres, T. *Chem. Commun.* **2001**, 399−400. (c) González-Cabello, A.; Vázquez, P.; Torres, T.; Guldi, D. M. *J. Org. Chem.* **2003**, *68*, 8635−8642.

(9) Echegoyen, L.; Echegoyen, L. E. *Acc. Chem. Res.* **1998**, *31*, 593−601.

(10) (a) *The Chemistry of the Fullerenes*; Hirsch, A., Ed.; Georg Thieme Verlag: Stuttgart, 1994. (b) *Science of Fullerenes and Carbon Nanotubes*; Dresselhaus, M. S., Dresselhaus, G., Eklund, P. C., Eds.; Academic Press: San Diego, CA, 1996. (c) *Fullerenes: from Synthesis to Optoelectronic Properties*; Guldi, D. M., Martín, N., Eds.; Kluwer Academic Publishers: Dodrech, 2002.

(11) (a) Imahori, H.; Sakata, Y. *Adv. Mater.* **1997**, *9*, 537−546. (b) Prato, M. *J. Mater. Chem.* **1997**, *7*, 1097−1109. (c) Martín, N.; Sánchez, L.; Illescas, B.; Pérez, I. *Chem. Rev.* **1998**, *98*, 2527−2547. (d) Diederich, F.; Gómez-López, M. *Chem. Soc. Rev.* **1999**, *28*, 263−277. (e) Imahori, H.; Sakata, Y. *Eur. J. Org. Chem.* **1999**, 2445−2457. (f) Guldi, D. M. *Chem. Commun.* **2000**, 321−327. (g) Guldi, D. M.; Prato, M. *Acc. Chem. Res.* **2000**, *33*, 695−703. (h) Reed, C. A.; Bolskar, R. D. *Chem. Rev.* **2000**, *100*, 1075−1120. (i) Gust, D.; Moore, T. A.; Moore, A. L. *J. Photochem. Photobiol., B* **2000**, *58*, 63−71. (j) Gust, D.; Moore, T. A.; Moore, A. L. *Acc. Chem. Res.* **2001**, *34*, 40−48. (k) Guldi, D. M. *Chem. Soc. Rev.* **2002**, *31*, 22−36.

(12) (a) Linssen, T. G.; Durr, K.; Hanack, M.; Hirsch, A. *J. Chem. Soc. Chem. Commun.* **1995**, 103−104. (b) Durr, K.; Fiedler, S.; Linssen, T.;

Hirsch, A.; Hanack, M. *Chem. Ber.* **1997**, *130*, 1375−1378. (c) Sastre, A.; Gouloumis, A.; Vázquez, P.; Torres, T.; Doan, V.; Schwartz, B. J.; Wudl, F.; Echegoyen, L.; Rivera, J. *Org. Lett.* **1999**, *1*, 1807−1810. (d) Martínez-Díaz, M. V.; Fender, N. S.; Rodríguez-Morgade, M. S.; Gómez-López, M.; Diederich, F.; Echegoyen, L.; Stoddart, J. F.; Torres, T. *J. Mater. Chem.* **2002**, *12*, 2095−2099. (e) Guldi, D. M.; Ramey, J.; Martínez-Díaz, M. V.; de la Escosura, A.; Torres, T.; Da Ros, T.; Prato, M. *Chem. Commun.* **2002**, 2774−2775. (f) González-Rodríguez, D.; Torres, T. In *The Exciting World of Nanocages and Nanotubes;* Kamat, P., Guldi, D. M., Kadish, K., Eds.; Proc. Electrochem. Soc., Fullerenes; ECS: Pennington, NJ, 2002; Vol. 12, pp 195−210.

(13) Gouloumis, A.; Liu, S.-G.; Sastre, A.; Vázquez, P.; Echegoyen, L.; Torres, T. *Chem. Eur. J.* **2000**, *6*, 3600−3607.

(14) Guldi, D. M.; Gouloumis, A.; Vázquez, P.; Torres, T. *Chem. Commun.* **2002**, 2056−2057.

(15) Loi, M. A.; Neugebauer, H.; Denk, P.; Brabec, C. J.; Sariciftci, N. S.; Gouloumis, A.; Vázquez, P.; Torres, T. *J. Mater. Chem.* **2003**, *13*, 700−704.

(16) Stille, J. K. *Angew. Chem., Int. Ed. Engl.* **1986**, *25*, 508−524.

(17) Cainelli, G.; Contento, M.; Manescalchi, F.; Plessi, L. *Synthesis* **1989**, 47−48.

(18) No correction was applied that accounts for electrostatic interactions in the dyads.

(19) Kavarnos, G. J. *Fundamentals of Photoinduced Electron Transfer*; VCH−Wiley: New York, 1993.

(20) Guldi, D. M.; Prato, M. *Acc. Chem. Res.* **2000**, *33*, 695−703.

(21) (a) Armaroli, N.; Marconi, G.; Echegoyen, L.; Bourgeois, J.-P.; Diederich, F. *Chem. Eur. J.* **2000**, *6*, 1629−1645. (b) Imahori, H.; Tkachenko, N. V.; Vehmanen, V.; Tamaki, K.; Lemmetyinen, H.; Sakata, Y.; Fukuzumi, S. *J. Phys. Chem. A* **2001**, *105*, 1750−11756.

(22) (a) Smith, B. E.; Gouterman, M. *Chem. Phys. Lett.* **1968**, *2*, 517−519. (b) Asano-Someda, M.; Sato, S.-I.; Aoyagi, K.; Kitagawa, T. *J. Phys. Chem.* **1995**, *99*, 13800−13807. (c) Asano-Someda, M.; Kaizu, Y. *Photochem. Photobiol., A* **1995**, *87*, 23−25.

(23) (a) Oevering, H.; Paddon-Row: M. N.; Heppner, M.; Oliver, A. M.; Cotsaris, E.; Verhoeven, J. W.; Hush, N. S. *J. Am. Chem. Soc.* **1987**, *109*, 3258−3269. (b) Marcus, R. A. *J. Phys. Chem.* **1989**, *93*, 3078−3086.

(24) We still see the singlet transient.

(25) (a) Marcus, R. A. *Annu. Rev. Phys. Chem.* **1964**, *15*, 155−159. (b) Marcus, R. A. *Angew. Chem., Int. Ed. Engl.* **1993**, *32*, 1111−1121.

(26) (a) Fukuzumi, S. *Org. Biomol. Chem.* **2003**, *1*, 609−620. (b) Kashiwagi, Y.; Ohkubo, K.; McDonal, J. A.; Blake, I. M.; Crossley, M. J.; Araki, Y.; Ito, O.; Imahori, H.; Fukuzumi, S. *Org. Lett.* **2003**, *5*, 2719−2721. (c) Ohkubo, K.; Kotani, H.; Shao, J. G.; Ou, Z. P.; Kadish, K. M.; Li, G. L.; Pandey, R. K.; Fujitsuka, M.; Ito, O.; Imahori, H.; Fukuzumi, S. *Angew. Chem. Int. Ed.* **2004**, *43*, 853−856.